Thermal Image-Based Solar PV Fault Detection Leveraging YOLOv5 Model Variants

Nurul Faqihah Hambali[1], A. R. Syafeeza[1*], Ridza Azri Ramlee[1], Muhammad Izzaham Faddlie Zahari[2], Muhammad Farhan Norazman[2]

[1]*Faculty of Electronics & Computer Technology and Engineering, Universiti Teknikal Malaysia Melaka, Hang Tuah Jaya, Durian Tunggal, Melaka, Malaysia*
[2]*Neometra Synergy Sdn Bhd, D806 Block D, Kelana Square, Jala S57/26, Kelana Jaya, 47301 Petaling Jaya, Selangor, Malaysia*

Article Info	Abstract
	This paper analyzed the performance of deep learning model variant of YOLOv5 for fault detection in solar photovoltaic (PV) systems using infrared thermography images. The explosive growth of solar PV energy globally has posed challenges in maintaining these systems. Traditional maintenance methods rely on manual on-site inspection, which are time-consuming - particularly for large numbers of solar panels - and may cause delays in maintenance work. To overcome these issues, Artificial Intelligence (AI) is utilized to develop automated and real-time solar PV fault detection using infrared thermal images. This paper investigates variants of deep learning techniques, specifically the YOLO architecture, in solar PV fault detection across eight classes using YOLOv5s, YOLOv5m, and YOLOv5l models. The eight fault classes considered in this study are: cell, multi-cell, shading, string, substring, reverse polarity, module and junction box. The training results and evaluation metrics were carefully examined to identify the most effective model. The YOLOv5l model emerged as the top-performing option, demonstrating superior detection accuracy, localization accuracy, class prediction accuracy, precision, recall, and mean average precision (mAP). The overall accuracy percentages for the YOLOv5s and YOLOv5m models were 46.67% and 51.50%, respectively. YOLOv5l achieved 53.40% accuracy, showing a clear improvement compared to the YOLOv5s and YOLOv5m models. Hence, this study highlights the potential of YOLOv5l model for detecting solar PV faults across eight classes using infrared thermography images.

*Corresponding Author: syafeeza@utem.edu.my

I. INTRODUCTION

The rapid growth of global solar photovoltaic (PV) generation, serving as an alternative to conventional fossil fuel generation, is primarily driven by the installation of large-scale solar PV energy power plants [1], [2] . This growth highlights the necessity for modern solar plants equipped with new maintenance techniques to ensure more efficient and reliable operation and maintenance practices[3]. Condition monitoring systems play a pivotal role in enhancing reliability, reducing costs, and improving solar plant operation. However, monitoring renewable energy assets in these large plants remains challenging due to various faults that could diminish power generation, leading to malfunctioning and accelerating asset degradation. Moreover, misdiagnosing such faults may further complicate maintenance work and result in ineffective solutions.

To address these difficulties, advanced techniques such as the use of unmanned aerial vehicles (UAVs) or drones equipped with thermal imaging technology have been employed[4]. These drones capture thermal images and store them in Secure Digital (SD) cards, facilitating the detection of extended areas, enabling rapid data collection, and allowing assessment of installations in difficult-to-reach locations. The thermal images of the solar PV indicate the panel condition, highlighting heat conditions and other faults [5]. Additionally, by integrating deep learning algorithms, these thermal images can be analyzed to automatically detect and classify faults [6], thereby enhancing the accuracy and efficiency of solar PV system maintenance while minimizing the need for manual inspection.

The main objective of this study is to analyze the performance of deep learning models for the task of fault detection that can accurately categorize the faults in infrared thermography images into their respective types. There are eight types of faults, which are cell, multi-cell, shading, string, substring, reverse polarity, module and junction box. Accurate solar PV fault detection is crucial for effective monitoring and management, as it saves time and resources while enhancing accuracy and scalability. The significance of AI in this domain lies in its capacity to automate and improve

the effectiveness of these procedures, reducing the reliance on manual identification [6], [7], [8].

This study utilized the YOLOv5 model for solar PV fault detection. The YOLO architecture is known for its ability to perform real-time object detection with high accuracy, processing entire images quickly and efficiently. Thus, this approach presents an intriguing opportunity to address the problem of solar PV fault detection.

II. LITERATURE REVIEW

This section explores the overview of solar PV. The type of solar PV fault features plays a crucial role in extracting them from images. Besides, this section also reviews the YOLO model for solar PV fault detection.

A. Overview of Solar PV

Renewable energy sources, such as solar, are expected to drive a significant proportion of global power generation capacity, accounting for 75%–80% of newly installed capacity by 2050 [9] . In August 2023, Malaysia revised its target for renewable energy installed capacity from 40% by 2040 to 70% by 2050. Solar photovoltaic (PV) installations alone are expected to contribute to more than half of that growth. In numerous countries, the prevailing trend involves developing larger installations with power capacities reaching several tens or even hundreds of megawatts [10].

The growing installation of photovoltaic (PV) plants in Malaysia is due to several advantages of PV. PV power generation technology directly converts solar energy into clean, pollution-free electricity, which is widely promoted. The widespread adoption of solar PV power generation technology can significantly reduce the use of fossil fuels and environmental pollution. PV energy generation has experienced exponential growth in the last decade [11]. This growth is primarily driven by the installation of large-scale solar PV power plants, making significant strides towards achieving sustainable energy goals. This aligns with UN Sustainable Development Goals number 7, which promotes affordable and clean energy [12]. Solar energy plays a vital role in increasing access to affordable and clean energy. Since the solar cell can generate electricity from the sun, it is able to provide electricity in remote areas that are not connected to the grid.

B. Type of Solar PV Faults

Managing large solar installations requires high cost and is time-consuming for manual monitoring of solar panels. The difficulties of remote access futher complicate the task of reaching distant locations. Regular maintanence is essential for the sustainable management of solar plants, helping to extend their lifespan and improve performance. Faulty panel can affect the entire array's generation, leading to production losses of up to 20%. Efficient maintenance addresses various fault occurrences that diminish operational efficiency and pose safety risks. These faults within PV systems can be categorized as physical, environmental, or electrical faults [13], as illustrated in Table 1.

Table 1
Classification of faults [13], [14]

Types of faults	Description
Physical faults	i. Panel faults: PV cell internal damages, cracks in panels, bypass diodes, degradation faults, hotspots, corrosion in module, and broken panels
	ii. Inverter failure: manufacturing/ design failure, control problems, electrical component failure
Environmental faults (shading)	Bird dropping, vegetation, dust accumulation, cloud movement, and tree shadows
Electrical faults	MPPT faults, open-circuit faults, ground faults, line-line faults, short-circuit faults, arc faults, and islanding operation

C. Fault Detection Using Infrared Thermography Images

Infrared thermography (IRT) is particularly popular due to its non-invasive nature and contactless technique. The application of infrared thermography lies in its ability to measure the superficial temperature of objects based on radiation emitted in the thermal infrared band of the spectrum. Besides, IRT is widely used because it provides fast, reliable, accurate and cost-effective two-dimensional representations of distinctive attributes of PV modules [15]. Additionally, thermography is a useful method for identifying and classifying faults in PV modules.

Furthermore, solar PV system faults can also be detected through thermal image inspection, which facilitates the identification of temperature anomalies, such as hotspots, that may indicate potential defects or inefficiencies in the system. By analyzing thermal patterns, issues such as shading effects, reverse polarity, or damaged cells can be identified quickly and accurately, thereby enhancing fault diagnosis and system maintenance. In this study, there are eight classes of faults: cell, multi-cell, shading, string, substring, reverse polarity, module and junction box. For instance, reverse polarity faults can be detected in thermal images of solar PV panels. When a reverse polarity fault occurs, it can lead to abnormal heating patterns in the solar cells or connections, which may be visible in thermal images. This can be seen in Figure 1 below.
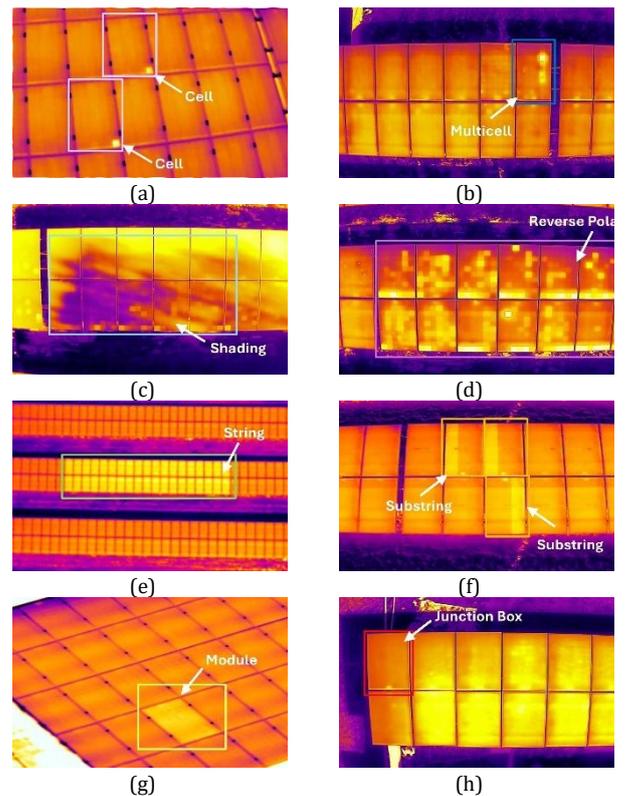

Figure 1. Thermal images of solar PV fault detection (a)cell, (b)multicell, (c)shading, (d)reverse polarity, (e)string, (f) substring, (g)module and (h)junction-box.

D. *You Only Look Once (YOLO) Model Architecture*

YOLOv5 consists of three parts: (1) backbone, (2) neck and (3) detect/head. It utilizes a CSPDarknet backbone, a Path Aggregation Network (PAN) and a Feature Pyramid Network (FPN) neck, and three detection heads for accurate bounding box prediction. The architecture includes various convolutional layers (Conv), concatenation layers (Concat), and upsampling layers (Upsample), culminating in detection layers that output bounding box coordinates, objectness scores, and class probabilities. This intricate structure enables the model to capture detailed features and perform accurate detections. This architecture is designed to achieve high accuracy and fast processing speed [16], [17]. YOLOv5 is also offered in multiple size variants, such as YOLOv5s, YOLOv5m, YOLOv5l, YOLOv5x. The model size can be adjusted by changing the depth and width values of the model. As a result, YOLOv5 is useful for a wide range of applications. The architecture of YOLOv5 is depicted in Figure 2.
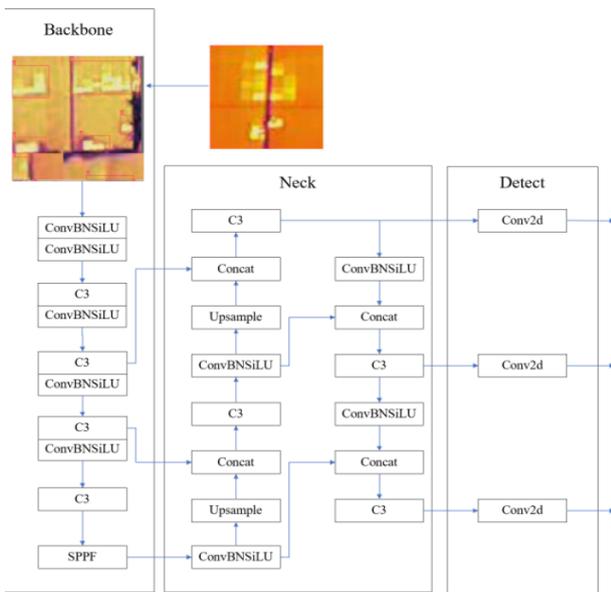
Additionally, Liang et al. (2023) [18] conducted research on a thermal-based inspection for photovoltaic panels employing the YOLOv5 model. The study achieved a precision rate of 75.4%, a recall rate of 69.6%, a mean Average Precision (mAP) @0.5 value of 69.7%, and a mAP@ 0.5:0.95 value of 27.4% [18]. In this study, the experiment conducted was primarily for a single class of faults. Furthermore, Zheng et al. (2023)[19] researched surface defect detection in solar cells using YOLOv5 model. The study reported a mean Average Precision (mAP) @0.5 of 95.6% [19]. However, this high performance was also limited to a single class of surface defects.

Overall, these results demonstrate that the YOLOv5 model achieves excellent accuracy for single-fault detection. Hence, this study aims to investigate the performance of YOLOv5 model variants when applied to multiple fault classes in solar PV systems. By expanding the number of fault categories, the study will provide deeper insights into the scalability of YOLOv5 model variants in solar PV fault detection task. Thus, the comparison between the different YOLOv5 model variants can be discussed further.

III. METHODOLOGY

In this section of the study, the faults of solar PV infrared thermal images are detected using the YOLOv5 deep learning model. The simulation is carried out using Google Colab. Google Colab, short for Google Colaboratory, is a cost-free, cloud-based Jupyter notebook platform used to train, validate and test the data of the solar PV fault infrared thermal image data.

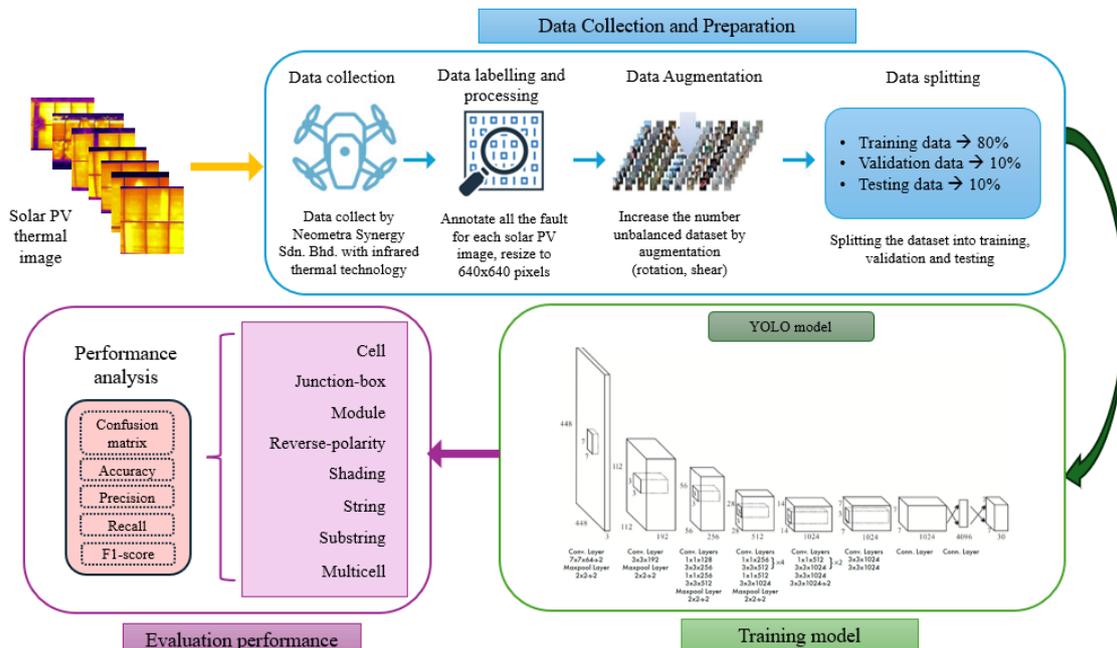Figure 2. YOLOv5 basic structure architecture [18]

Figure 3. Outline for the methodology

In addition, a web-based software known as Roboflow is employed to accomplish the remaining tasks in the dataset preparation stage. Roboflow is a specific software tool designed to simplify and streamline the process of working with computer vision datasets for training machine learning and deep learning models. Figure 3 illustrates the outline of this study. The methodology comprises three sequential stages: (1) data collection and preparation, (2) training with YOLOv5 models, and (3) evaluation and analysis the performance.

A. Data Collection and Preparation

This stage involves four procedures: data collection, data labelling and processing, data augmentation and data splitting. Firstly, the process begins with the collection of thermal images of solar PV panels, with the dataset provided by Neometra Synergy Sdn. Bhd. Due to the proprietary nature of this data, it cannot be shared with the public. Moreover, this dataset was captured using a drone equipped with thermal imaging technology. Specifically, the MAVIC 3 Enterprise drone, developed by Da Jiang Innovation (DJI), was employed for this study. The MAVIC 3 drone offers significant advantages, including an integrated high-resolution thermal imaging sensor that enables rapid object recognition in the field. The dataset includes thermal images representing eight different types of faults: cell, multi-cell, shading, string, sub-string, reverse polarity, module, and junction box faults. A total of 605 fault images had been collected.

Next, the procedure continues with data labelling and data processing stage. Before inputing the images into deep learning model, the thermal images undergo several steps, such as data labelling, and annotation. This process is important for training accurate deep learning models and is executed by using Roboflow. Each fault is annotated with precise bounding boxes, which indicates the fault's location within the image. This directly influences the deep learning model's capacity to learn and effeciently identify faults in solar PV systems. This is shown in Figure 4.
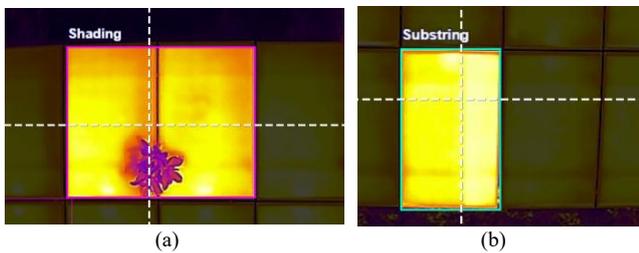

Figure 4. Labelling data in the Roboflow (a) shading and (b) substring

A total of 605 thermal images were collected from Neometra Synergy Sdn Bhd. However, the number of images does not match the number of annotations because some thermal images have more than one annotation, leading to a higher count of annotations compared to the number of images. In other words, one image has multilabel, which is multiple classes in a single image. For example, a single thermal image of a solar PV panel might be labelled with different types of faults such as substring, cell and multi-cell, indicating the presence of multiple faults in that of image. This is shown in Figure 5.
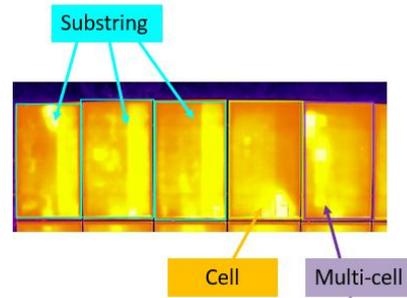

Figure 5. Multilabel classification of faults in solar PV panel thermal images

Hence, the total number of annotations obtained after the labelling process is 1,369. Table 2 illustrates the data distribution for each class of fault. From the data annotation and labelling earlier, it is evident that the distribution is imbalanced between fault classes, especially for shading and reverse polarity. These differences highlight the need for data augmentation techniques to ensure that the model performs consistently across all categories, particularly those with lower representation. Therefore, augmentation techniques, such as rotation, flipping and zooming are implemented to increase the datasets without the need to collect new data.

Table 2.
Number of annotations for each class

Classes	Total
Multicell	436
Cell	245
Module	199
Junction box	138
String	132
Substring	130
Shading	51
Reverse polarity	38
Total (annotations)	1369

Furthermore, the images undergo pre-processing. In this study, the dataset includes image with variations in size and width. It is necessary for all images to have uniform dimensions to achieve optimal classification findings. Therefore, the image must be resized before modelling. This study utilizes images with dimensions of 640x640 pixels. Once the images have been normalized, the dataset continues with data augmentation process. By implementing various transformations to the existing data, the model's generalization ability is enhanced and overfitting is prevented. In this research, geometric transformations are employed for data augmentation using Roboflow. This is illustrated in Figure 6.
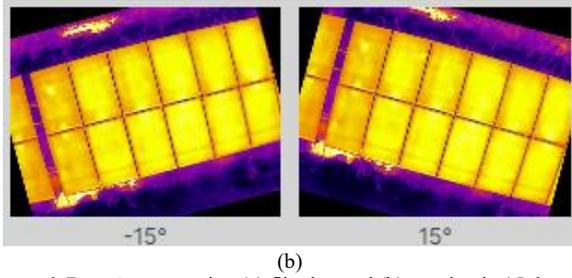

(a)

(b)
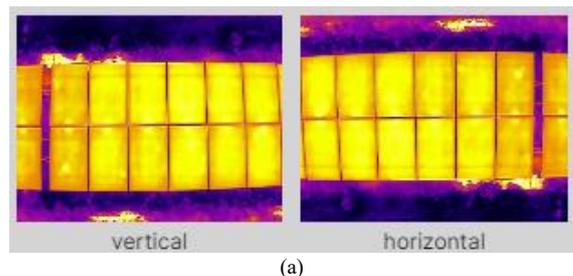
Figure 6. Data Augmentation (a) flipping and (b) rotation in 15 degrees

The selection of flipping and rotating augmentation techniques is based on the ability of drones to acquire images from several angles and orientations while going through the solar PV panels. These augmentations simulate the natural variations in perspective and orientation resulting from the drone's flight trajectory. This ensures the model's resilience to these fluctuations and its ability to accurately detect defects regardless of the drone's position. Hence, geometric transformation is a suitable augmentation method to improve the model's robustness, under varying imaging conditions. As a result, 1,184 images are produced at the end of data augmentation process.

Lastly, the procedure continues with data splitting. After those images undergo the data augmentation process, the dataset is split into training, validating and testing sets in a ratio of 80:10:10. Table 3 shows the distribution of the 1,184 images across each.

Table 3.
Data distribution between training, validation and testing sets

Sets	Number of images
Training	954
Validation	116
Testing	114
Total	**1184**

Furthermore, Roboflow automatically generates the configuration file, "data.yaml" for the solar PV fault infrared thermal image dataset. The dataset.yaml file contains information such as the paths to the training, validation, and testing image directories, the number of classes and their respective labels, and other dataset-specific settings, as illustrated in Figure 7. It also provides the necessary instructions and metadata required for the training script to locate and process the dataset correctly. In simple terms, it ensures the YOLOv5 training script can access the dataset effectively, load the images and annotations properly, and perform the necessary operations during the training process.

```
names:
-Cell
-Junction-Box
-Module
-Multicell
-Reverse-Polarity
-Shading
-String
-Substring
nc: 8
roboflow:
license: CC BY 4.0
project: solar-detection-ahe9h
url:  https://universe.roboflow.com/solar-uqyqu/solar-detection-
he9h/dataset/12
version: 12
```

```
workspace: solar-uqyqu
test: ./test/images
train: Solar-Detection-12/train/images
val: Solar-Detection-12/valid/images
```

Figure 7. "data.yaml" file for the solar PV fault infrared thermal image dataset

B. Model Training

The experiment continues with the second stage, which is training the deep learning model. As mentioned earlier, the objective is study to analyze the performance of YOLOv5 deep learning model variants for detecting eight classes of solar PV fault detection task based on infrared thermography images. Hence, to achieve this objective, the variants of the YOLOv5 family are implement at this stage, namely YOLOv5s (Small) model, YOLOv5m (Medium) model, and YOLOv5l (Large) model. All models implementations utilize different features in the network architecture. These variants represent different configurations and sizes of the YOLOv5 architecture. Therefore, training multiple models allows for a comparative analysis of their performance on the solar PV fault detection task.

The installation of YOLOv5 model weight must be executed in the Google Colab to enable the training process. The YOLO models can be downlaoded directly from the Ultralytic Github repository. This is shown in Figure 8.

```
# clone YOLOv5 repository
!git clone https://github.com/ultralytics/yolov5  # clone repo
%cd yolov5
!git reset --hard 064365d8683fd002e9ad789c1e91fa3d021b44f0

Cloning into 'yolov5'...
remote: Enumerating objects: 16675, done.
remote: Counting objects: 100% (216/216), done.
remote: Compressing objects: 100% (157/157), done.
remote: Total 16675 (delta 98), reused 127 (delta 59), pack-reused 16459
Receiving objects: 100% (16675/16675), 15.32 MiB | 12.61 MiB/s, done.
Resolving deltas: 100% (11404/11404), done.
/content/yolov5
HEAD is now at 064365d8 Update parse_opt() in export.py to work as in train.py (#10789)
```

Figure 8. Installation on YOLOv5 algorithm in Google Colab

Before the training process of the YOLOv5s, YOLOv5m YOLOv5l models can be initiated, the configuration files of these models need to be customized because the models differ in terms of depth and width values. The difference configuration of the YOLOv5 variants are shown in Table 4.

Table 4.
Difference configuration of YOLOv5 model variants

Model	Depth Multiple	Width Multiple	Parameters	Layers
YOLOv5s	0.33	0.50	7,041,205	214
YOLOv5m	0.67	0.75	20,899,605	291
YOLOv5l	1.0	1.0	46,175,989	368

Besides that, adjustments to hyperparameter values are necessary, as they significantly influence the learning process during model training and subsequently affect the model's performance. The specific hyperparameters used are detailed in Table 5.

In this experiment, the hyperparameter values for all YOLOv5 models (s, m, and l) were kept consistent: a batch size of 16, 8 classes, and a learning rate of 0.01. The backpropagation process employs the Stochastic Gradient Descent (SGD) optimizer, with the momentum parameter set to 0.937 to enhance the model's convergence rate. The training process consists of 500 iterations. The number of

training rounds is determined by evaluating the model's performance on the validation dataset and analyzing the training process to identify the optimal point for achieving the best results.

Then, the training process for the YOLOv5s, YOLOv5m, and YOLOv5l models is initiated using specific commands tailored to each model. For the YOLOv5s model, the command used to initiate the training is shown in Figure 9 below.

Table 5.
Training parameter for YOLOv5 model variants

Hyperparameters	YOLOv5
Image Size	640x640
Batch Size	16
Class	8
Learning rate	0.01
Optimizer	SGD
Momentum	0.937
Number of epochs	500

```
!python train.py  --img 640  --batch 16  --epochs 500 --data
{dataset.location}/data.yaml
--cfg  ./models/custom_yolov5s.yaml  --weights  ' '  --name
yolov5s_results_500
```

Figure 9. The command used to initiate the YOLOv5s model training.

C. Performance Analysis

During this stage, the trained models are evaluated by comparing the accuracy of the training and validation processes. The evaluation of the training involves assessing key performance metric such as accuracy, precision and recall, and mean Average Precision (mAP) to ascertain the efficiency of the models. The following parameters are calculated in the evaluation metric.

- True Positive (TP): The number of solar PV infrared thermal fault image samples (e.g.: substring) correctly classified.
- True Negative (TN): The number of other fault class samples correctly labelled as not belonging to the target class.
- False Positive (FP): A false positive occurs when substring fault class is misclassified as another fault class.
- False Negative (FN): Other fault classes that are mislabelled as substring.

These parameters can be obtained from the confusion matrix, as shown in Figure 10. A confusion matrix is a valuable tool for assessing the effectiveness of a classification model by comparing the actual and predicted values.

In this study, there are eight classification classes. Each class will have its own parameters values, which are distributed throughout the matrix. The confusion matrix is a symmetrical matrix in which each row corresponds to the true class, and each column corresponds to the predicted class. The diagonal elements correspond to the accurately classified instances for each class. The classification report can be obtained from the confusion matrix. It includes metrics such as, precision, recall, F1-score and mAP. These metrics can be computed to assess the performance of the model and offer valuable information about the model's proficiency in accurately classifying the classes.
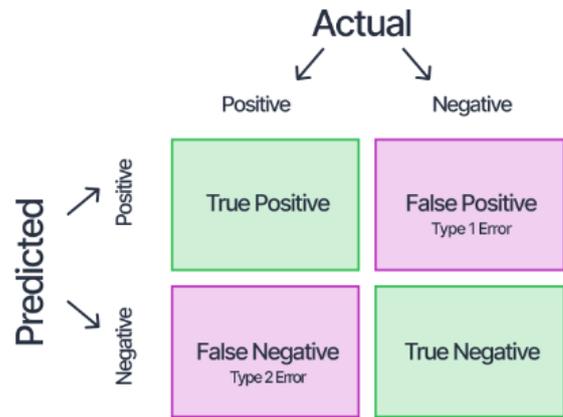

Figure 10. Basic binary classifications confusion matrix [15]

The metrics for each class are calculated as follows, involving the use of confusion matrix:

Precision: This metric measures the level of correctness in positive predictions.

$$precision = \frac{TP}{TP + FP} \qquad (1)$$

- Recall: The metric measures the ability of the model to classify all instances of the positive class.

$$recall = \frac{TP}{TP + FN} \qquad (2)$$

- mAP (Mean Average Precision): This metric calculates the average precision for each class and averages it over all classes, combining precision and recall into a single value.

$$mAP = \frac{1}{n} AP = \frac{1}{n} \sum_{k=1}^{k=n} AP_k \qquad (3)$$

where: AP_k = the AP of class k
n = number of classes.

In addition, mAP can be evaluated at various Intersection over Union (IoU) thresholds. This assessment helps to measure the model's performance at different levels of detection accuracy [20]. By calculating mAP at different IoU levels, such as 0.5 and 0.95, it is possible to assess the models' ability to precisely locate objects under varied levels of overlap between predicted and actual bounding boxes. Overall, metric values are essential for evaluating object detection models. In this research, the performance of YOLOv5s, YOLOv5m and YOLOv5l is assessed in detecting faults in solar PV system. The model performance of this study is described in the next section.

IV. RESULT AND DISCUSSION

This section presents the findings of the YOLOv5 model variants on the solar PV fault infrared thermal image dataset. The primary goal of this study is to investigate performance of YOLOv5 models for the fault detection task that can accurately categorize faults based on infrared thermography images into their respective types of faults. The simulations

were executed on Google Colab, leveraging the Ultralytics GitHub repository for the YOLOv5 models. This section also includes a performance evaluation for YOLOv5s, YOLOv5m and YOLOv5l model. A comparison is then made between the three models.

A. Simulation Setup

The experiment was conducted utilizing Google Colab, a cloud-based system equipped with an Intel(R) Core (TM) i7-11800H CPU running at a base clock of 2.30GHz and 8.0 GB RAM. The solar PV fault infrared thermal image dataset was obtained from the Neometra Synergy Sdn. Bhd.

B. Model Performance.

1) YOLOv5s Model

The YOLOv5s model was implemented to train the solar PV fault infrared thermal images. The training process for YOLOv5s stopped at 458 epochs and took approximately 2,518 hours.

Figure 11. Confusion matrix of YOLOv5s model

Figure 11 illustrates the confusion matrix, which evaluates the ability of a YOLOv5s model to accurately differentiate between eight fault classes. The matrix displays true labels on the y-axis and predicted labels on the x-axis. Diagonal elements represent correctly classified instances, with high values indicating strong performance in certain categories, such as for "module" class, which shows a value of 0.59. However, off-diagonal elements represent misclassifications, highlighting areas for improvement. For example, the "multicell" class is sometimes misclassified as "cell", "shading", "string", and "background," with a significant value of 0.21. This visualization helps identify which specific classes are often confused with others. From the confusion matrix, a classification report is generated, as shown in Table 6.

Table 6.
YOLOv5s model training report

Class	P	R	mAP:50	mAP:50-95
Cell	0.543	0.500	0.507	0.376
Junction-box	0.680	0.436	0.522	0.446
Module	0.728	0.607	0.649	0.498
Multicell	0.608	0.705	0.729	0.553
Reverse-polarity	0.858	0.671	0.807	0.436
Shading	0.855	0.500	0.812	0.205
String	0.710	0.436	0.506	0.247
Substring	0.705	0.717	0.873	0.762
Overall	0.711	0.572	0.638	0.441

Table 6 presents a classification report that includes precision (P), recall (R), and mean Average Precision (mAP) for each of the eight fault classes: cell, multi-cell, shading, string, sub-string, reverse polarity, module, and junction box. Performance metrics vary across classes, with "module" showing the highest precision (0.728) and "reverse-polarity" exhibiting the highest recall (0.858). The overall mean average precision at IoU 0.5 (mAP50) is 0.638, with the highest for "Reverse-polarity" at 0.807. The mean average precision across IoU thresholds (mAP50-95) is 0.441, indicating a reasonable level of performance but highlighting areas for improvement. These metrics highlight that the YOLOv5s model's balanced performance across different solar PV faults.

2) YOLOv5m Model

The solar PV fault infrared thermal image classification continues with another version of YOLOv5 series, which is YOLOv5m model. This model aims to improve the performance of image classification in terms of accuracy. The YOLOv5m model's stopped training at 427 epochs, which less than YOLOv5s model and took approximately 3.487 hours.

Figure 12. Confusion matrix of YOLOv5m model

Figure 12 presents a confusion matrix that assesses the performance of the YOLOv5m model. The diagonal cells, where predicted and true classes match, indicate correct predictions, with darker blue shades indicating higher accuracy. For example, the "cell" class has a diagonal value of 0.52 on the diagonal, indicating 52% accuracy. On the other hand, the "multicell" has a high accuracy of 0.77, and the "reverse polarity" class shows a very high accuracy of 0.89. However, the off-diagonal cells indicate misclassification faults. For example, "multicell" is misclassified as "background" (0.21), "junction-box" (0.03), "module" (0.02), "shading" (0.37) and "substring" (0.10).

Table 7.
YOLOv5m model report classification

Class	P	R	mAP:50	mAP:50-95
Cell	0.568	0.538	0.505	0.378
Junction-box	0.630	0.262	0.380	0.325
Module	0.801	0.640	0.682	0.495
Multicell	0.733	0.748	0.736	0.571
Reverse-polarity	0.513	0.889	0.710	0.235
Shading	0.489	0.375	0.454	0.251
String	0.627	0.385	0.419	0.235
Substring	0.893	0.834	0.940	0.754
Overall	0.657	0.584	0.603	0.406

Table 7 shows the classification report for the YOLOv5m model. The YOLOv5m model's performance metrics reveal variability across different classes. "Substring" stands out with the highest precision (0.893), recall (0.834), mAP@0.50 (0.940), and mAP@0.50:0.95 (0.754), indicating strong model performance. Conversely, "junction-box" and "shading" show weaker results, with "junction-box" having the lowest recall (0.262) and mAP@0.50 (0.380), and "shading" the lowest precision (0.489). Overall, the classification report indicates that the YOLOv5m model's precision is 0.657, recall is 0.584, mAP@0.50 is 0.603, and mAP@0.50:0.95 is 0.406. This suggests the model performs well in several classes, though improvements are needed to achieve a more balanced performance across all categories.

3) YOLOv5l Model

The YOLOv5l model then is implemented to train the solar PV fault infrared thermal image. Figure 13 displays the complete training process of the YOLOv5l model with 500 epochs. However, the training process stopped at 468 epochs and took approximately 5.775 hours. As the version of the model increases, the longer time is needed to complete the training process.

Figure 13. Confusion matrix of YOLOv5l model

Next, Figure 13 illustrates the confusion matrix that evaluates the ability of the YOLOv5l model to accurately predict the eight different fault classes. The most accurately predicted fault classes are "reverse polarity" and "substring", with 0.89 and 0.80 correct predictions respectively. Misclassification is still present in the confusion matrix. However, the values are

slightly reduced compared to the YOLOv5m model. For example, "multicell" is frequently misclassified as "cell" and "junction box". Initially, the misclassification of "cell" with YOLOv5s was 0.25. Then, it reduced to 0.22 with YOLOv5m and by implementing YOLOv5l model, the value decreased to 0.17. This indicates that the error for misclassification is decreasing. Overall, the confusion matrix shows that the YOLOv5l model is able to classify the fault images more accurately and improves accuracy compared to the YOLOv5s and YOLOv5m models.

Table 8.
YOLOv5l model training report

Class	P	R	mAP:50	mAP:50-95
Cell	0.552	0.462	0.501	0.372
Junction-box	0.505	0.34	0.425	0.371
Module	0.753	0.623	0.683	0.516
Multicell	0.734	0.750	0.762	0.574
Reverse-polarity	0.451	0.889	0.510	0.269
Shading	0.476	0.375	0.374	0.124
String	0.679	0.487	0.541	0.282
Substring	0.821	0.900	0.968	0.837
Overall	0.621	0.603	0.596	0.418

Table 8 presents the YOLOv5l model classification report that includes precision, recall, and mAP for the model tested on eight classes. "Substring" has the highest scores with precision at 0.821, recall at 0.9, mAP@0.50 at 0.968, and mAP@0.50:0.95 at 0.837, indicating exceptional performance. In contrast, "junction-box" shows low performance with precision at 0.505 and recall at 0.34, while "shading" records the lowest mAP@0.50 (0.374) and mAP@0.50:0.95 (0.124). Overall, the model achieved a precision of 0.621, recall of 0.603, mAP@0.50 of 0.596, and mAP@0.50:0.95 of 0.418. These metrics highlight the YOLOv5l model's balanced performance across different solar PV fault classes. However, some specific classes such as "junction-box" and "shading" still require improvement.

C. Comparison Between YOLOv5s, YOLOv5m, and YOLOv5l Models

The purpose of this study is to evaluate the performance of various YOLOv5 model variants (YOLOv5s, YOLOv5m, and YOLOv5l) in identifying eight different fault classes. By training the infrared thermography image data on these YOLOv5 variants, the best-performing the fault detection model across all eight classes was determined. A comparison of the results from the three variants shows that YOLOv5l achieves the highest overall accuracy. The detailed performance comparison of the three YOLOv5 model variants (YOLOv5s, YOLOv5m, and YOLOv5l) is summarized in Table 9.

Table 9 shows that the YOLOv5s model from other authors[18], [19] achieved high performance value, but only for a single class. To further evaluate the capability of YOLOv5 for multiclass detection, this study investigates the performance of three YOLOv5 model variants (YOLOv5s, YOLOv5m, and YOLOv5l) on eight fault classes.

In addition, Table 9 highlights the training times, precision, recall, mean average precision(mAP) at different IoU thresholds and overall accuracy. From the simulation findings the results show that as the model complexity increases, the

training time also increases. Training time increases with model size, from 2.158 hours for YOLOv5s to 5.775 hours for YOLOv5l. Although YOLOv5s is the fastest to train, it achieves lower accuracy compared to YOLOv5m and YOLOv5l. YOLOv5l outperforms the other two in terms of precision, recall, and overall accuracy. In particular, YOLOv5l model able to identify eight classes of fault with the highest value compared to the other two models, which is 53.4%. This comparison provides valuable insights into the trade-offs between training time, precision, recall, and detection performance, aiding in selecting the most suitable model variant based on specific application needs and computational resources.

Moreover, the YOLOv5l model achieves the highest training accuracy values among the three models across the 500-epochs training process. This implies that YOLOv5l model exhibits superior object localization and classification capabilities compared to the YOLOv5s and YOLOv5m models. The enhanced performance of the YOLOv5l model is likely due to its larger architecture and greater number of parameters, enabling it to capture more intricate features and nuances in the images. The larger architecture and increased number of parameters in the YOLOv5l model indicate that it has a more complex structure, with a deeper and wider network structure. With more parameters, the YOLOv5l model is able to identify finer details and patterns in the data, which plays a vital role in detecting fault based on infrared thermography images. Hence, the YOLOv5l model has achieved higher accuracy compared to other variant models.

Furthermore, the overall accuracy of 53.4% may seem low, but this is due to several factors. Since the model must differentiate between multiple categories, detecting eight classes is more difficult than detecting a single class using infrared thermography images. Therefore, while it may be possible to train the model with grayscale images, standard visual images of solar PV systems are generally insufficient for detecting the necessary patterns and anomalies. This makes thermal images essential for accurate condition monitoring. In addition, YOLOv5 variants might not be able to handle complicated datasets well. Performance could be improved by employing larger models such as YOLOv9, YOLOv10 or YOLOv11, which are designed to handle more complex datasets with greater precision and efficiency. These newer variants typically have enhanced architectures, larger capacities, and improved optimization techniques that allow them to better model intricate patterns in data.

CONCLUSION

In conclusion, identifying solar PV faults based on infrared thermal image becomes more challenging due to factors such as heat pattern, thermal contrast, temperature distribution and shape and size of thermal anomalies. Hence, the main goal of this study is to classify the fault images with their respective types by implementing YOLOv5 models. Moreover, the evaluation of the training, which involves measuring accuracy, precision, recall, and mAP value was conducted to determine the effectiveness of the models in classifying solar PV faults based on infrared thermal images.

From the results obtained, the YOLOv5l model attained a high accuracy of 53.4% after training for 500 epochs compared to the YOLOv5s and YOLOv5l models, although it required a longer time to execute the process. This indicates that the YOLOv5l model is likely to possess greater

complexity and the ability to detect more complex patterns within the data. Therefore, the trade-off between accuracy and training time must be carefully considered when selecting a model for a specific task.

For future work in classifying solar PV fault images using YOLO, it is desirable to increase the number of datasets. This is due to the fact that the testing error decreases as the volume of data increases, enabling the model to generalize more effectively from a larger amount of information. In addition, the YOLOv5 model can be improved by integrating attention mechanisms into the architecture or creating hybrid models with other deep learning techniques. Furthermore, further research can be carried out using new versions of YOLO models such as YOLOv9, YOLOv10 or YOLOv11 to improve the accuracy of fault detection. By leveraging these new versions, it becomes possible to achieve higher detection accuracy and better handle the challenges posed by multi-class and complicated datasets. In summary, YOLOv5l variants achieved the highest accuracy compared to other variants in detecting fault of infrared thermography images.

ACKNOWLEDGMENT

CONFLICT OF INTEREST

Authors declare that there is no conflict of interest regarding the publication of the paper.

AUTHOR CONTRIBUTION

The authors confirm their contributions to the paper as follows: study conception and design were carried out by Nurul Faqihah Hambali and A. R. Syafeeza; data collection was conducted by Nurul Faqihah Hambali, A. R. Syafeeza, and Ridza Azri Ramlee; analysis and interpretation of findings were performed by A. R. Syafeeza, Muhammad Izzaham Faddlie Zahari, and Muhammad Farhan Norazman; and draft manuscript preparation was completed by Nurul Faqihah Hambali and A. R. Syafeeza. All authors have reviewed the findings and approved the final manuscript.

REFERENCES

[1] T. E. K. Zidane et al., "Grid-connected solar PV power plants optimization: a review," IEEE Access, vol. 11, pp. 79588–79608, 2023, https://doi.org/10.1109/ACCESS.2023.3299815

[2] X. Y. Li, X. Y. Dong, S. Chen, and Y. M. Ye, "The promising future of developing large-scale PV solar farms in China: a three-stage framework for site selection," Renew Energy, vol. 220, 2024, https://doi.org/10.1016/j.renene.2023.119638

[3] C. A. Ezeigweneme et al., "Smart grids in industrial paradigms: A review of progress, benefits, and maintenance implications," Engineering Science & Technology Journal, vol. 5, no. 1, pp. 1–20, 2024, https://doi.org/10.51594/estj/v5i1.719

[4] B. Kayci, B. E. Demir, and F. Demir, "Deep learning based fault detection and diagnosis in photovoltaic system using thermal images acquired by UAV," Politeknik Dergisi, vol. 27, no. 1, pp. 91–99, 2024, https://doi.org/10.2339/politeknik.1094586

[5]   S. Umar, M. S. Qureshi, and M. U. Nawaz, "Thermal imaging and AI in solar panel defect identification," International Journal of Advanced Engineering Technologies and Innovations, vol. 1, no. 3, pp. 73–95, 2024.

[6]   S. Prabhakaran, R. A. Uthra, and J. Preetharoselyn, "Deep learning-based model for defect detection and localization on photovoltaic panels," Computer Systems Science and Engineering, vol. 44, no. 3, pp. 2683–2700, 2023, https://doi.org/10.32604/csse.2023.028898

[7]   A. Mohammad, and F. Mahjabeen, "International Journal of Multidisciplinary Sciences and Arts Revolutionizing Solar Energy: The Impact of Artificial Intelligence on Photovoltaic Systems," vol. 2, no. 1, pp. 117–127, 2023.

[8]   T. Al Smadi, A. Handam, K. S. Gaeid, A. Al-Smadi, Y. Al-Husban, and A. S. Khalid, "Artificial intelligent control of energy management PV system," Results in Control and Optimization, vol. 14, 2024, https://doi.org/10.1016/j.rico.2023.100343

[9]   International Energy Agency, "International Energy Agency (IEA) World Energy Outlook 2022," Accessed: 20 Jan 2025, [Online.] Available: https://www.iea.org/reports/world-energy-outlook-2022

[10] J. Starzyński, P. Zawadzki, and D. Harańczyk, "Machine learning in solar plants inspection automation," Energies (Basel), vol. 15, no. 16, pp. 1–21, 2022, https://doi.org/10.3390/en15165966

[11] Y. Wang, Y. Shen, C. Li, K. Zhang, and H. Wei, "Hotspot detection of photovoltaic modules in infrared thermal image based on saliency analysis," in Proc. of the 34th Chinese Control and Decision Conference (CCDC 2022), 2022, pp. 1479–1484, https://doi.org/10.1109/CCDC55256.2022.10033497

[12] K. Obaideen et al., "On the contribution of solar energy to sustainable developments goals: case study on Mohammed bin Rashid Al Maktoum solar park," International Journal of Thermofluids, vol. 12, 2021, https://doi.org/10.1016/j.ijft.2021.100123

[13] D. S. Pillai and N. Rajasekar, "A comprehensive review on protection challenges and fault diagnosis in PV systems," Renewable and Sustainable Energy Reviews, vol. 91, pp. 18–40, 2018, https://doi.org/10.1016/j.rser.2018.03.082

[14] H. Bendale, H. Aswar, H. Bamb, P. Desai, and C. N. Aher, "Deep learning for solar panel maintenance: detecting faults and improving performance," in Proc. of 2023 14th International Conference on Computing Communication and Networking Technologies (ICCCNT 2023), 2023, pp. 1–5, https://doi.org/10.1109/ICCCNT56998.2023.10307465

[15] G. M. El-Banby, N. M. Moawad, B. A. Abouzalm, W. F. Abouzaid, and E. A. Ramadan, "Photovoltaic system fault detection techniques: a review," Neural Comput. Appl., vol. 35, no. 35, pp. 24829–24842, 2023, https://doi.org/10.1007/s00521-023-09041-7

[16] Z. Xie, H. Ma, W. He, J. Xu, and H. Wen, "YOLOv5-S2C2: an improved method of mask detection based on lightweight," IEEE Access, vol. 12, pp. 53306–53319, 2024, https://doi.org/10.1109/ACCESS.2024.3384230

[17] S. Lu, K. Wu, and J. Chen, "Solar cell surface defect detection based on optimized YOLOv5," IEEE Access, vol. 11, pp. 71026–71036, 2023, https://doi.org/10.1109/ACCESS.2023.3294344

[18] L. Liang, X. Wang, X. Li, and J. Xia, "Research on fault object detection method for photovoltaic panel UAV inspection based on YOLOv5," in Proc. of 2023 9th International Conference on Computer and Communications (ICCC 2023), 2023, pp. 1766–1770, https://doi.org/10.1109/ICCC59590.2023.10507623

[19] Q. Zheng, J. Ma, M. Liu, Y. Liu, Y. Li, and G. Shi, "Lightweight hot-spot fault detection model of photovoltaic panels in UAV remote-sensing image," Sensors, vol. 22, no. 12, 2022, https://doi.org/10.3390/s22124617

[20] A. N. Gajjar and J. Jethva, "Intersection over union based analysis of image detection/segmentation using CNN model," in Proc. of 2nd International Conference on Power, Control and Computing Technologies (ICPC2T 2022), 2022, pp. 1–6, https://doi.org/10.1109/ICPC2T53885.2022.9776896.